Cement and Concrete Composites 115 (2021) 103849

Contents lists available at ScienceDirect

Cement and Concrete Composites

journal homepage: http://www.elsevier.com/locate/cemconcomp

Using glass content to determine the reactivity of fly ash for thermodynamic calculations

Deborah Glosser [a,c,d], Prannoy Suraneni [b], O. Burkan Isgor [a,*], W. Jason Weiss [a]

[a] Civil and Construction Engineering, Oregon State University, Corvallis, OR 97331, USA
[b] Civil, Architectural, and Environmental Engineering, University of Miami, Coral Gables, FL 33146, USA
[c] College of Engineering and Design, Western Washington University, Bellingham, WA, 98225 USA
[d] Institute for Energy Studies, Western Washington University, Bellingham, WA, 98225, USA

ARTICLE INFO

Keywords:
Cement
Fly ash
Reactivity
Hydration
Pozzolanic reaction
Thermodynamic modeling

ABSTRACT

Thermodynamic models for the hydration of ordinary portland cement (OPC) typically predict the composition of the resulting pore solution and the hydrates well. However, predictions for cementitious systems containing OPC and supplementary cementitious materials (SCM) are more challenging. The bulk chemical composition of fly ash does not sufficiently reflect the reactive portion of the material, as the crystalline components of fly ash do not generally react in cementitious systems. Thermodynamic modeling inputs using only the bulk chemical composition of fly ash overestimate the extent of both pozzolanic and hydraulic reactions. Two additional approaches are presented to overcome this limitation. In the first approach, the maximum reactive fraction of fly ash is computed by multiplying each bulk phase of the fly ash by a degree of reaction (DoR*) that is measured experimentally through calorimetric methods. In the second approach, the reactive (glass) fraction of the fly ash is determined to calculate its reactivity. In this alternative approach, the fraction of crystalline oxides measured using quantitative x-ray diffraction (QXRD) is subtracted from bulk oxide content determined using x-ray fluorescence (XRF) to establish a degree of reaction for each phase (DoR_{ph}*) to be used in the determination of the thermodynamic modeling inputs. Thermodynamic modeling predictions substantially improve by incorporating fly ash reactivity into the calculations using either the DoR* or DoR_{ph}*. The calculation of the reactive phases of fly ash using QXRD and XRF data serve as a potential alternative to the current calorimetric methods to calculate reactivity.

1. Background and introduction

Thermodynamic modeling of ordinary portland cement (OPC) has proven to be a powerful tool for the prediction of pore solution composition (as well as its resistivity, pH, etc.) and solid reaction products [1–3]. Thermodynamic simulations can provide the data needed for engineers and researchers to design concrete mixtures optimized for performance for specific uses (such as bridge decks or parking garages) and particular environments (such as those where freeze-thaw resistance or corrosion resistance is needed) [1–5]. In OPC systems, when appropriate kinetic models and properly tuned thermodynamic databases are used, the bulk composition of the OPC provides sufficient inputs for thermodynamic calculations that are based on Gibbs Energy Minimization (GEMS) calculations [2,6]. However, predictions for cementitious systems containing OPC and supplementary cementitious materials (SCM) are more challenging [7]. This difficulty mainly originates from the uncertainty associated with the reactivity of fly ash, which is strongly influenced by both the chemical and structural composition, i.e., its crystal-to-glass ratio [8]. The bulk chemical composition of fly ash does not sufficiently reflect the reactive portion of the material, as the crystalline components of fly ash do not generally react in cementitious systems [9].

The reactivity of fly ash is determined by the total fraction of fly ash that has reacted at infinite time, i.e., the maximum amount of the ash that is capable of participating in chemical reactions in cement pastes [7,10]. Fly ash reactivity is critical for the strength [2], pore size refinement [3], and transport property development of OPC-fly ash systems. Fly ashes with a higher reactivity typically have improved strength development due to the formation of more calcium silicate hydrate (*C*–S–H) as a result of the pozzolanic reaction which is accompanied by a decrease in

* Corresponding author.
E-mail address: Burkan.isgor@oregonstate.edu (O.B. Isgor).

https://doi.org/10.1016/j.cemconcomp.2020.103849
Received 29 April 2020; Received in revised form 23 September 2020; Accepted 15 October 2020
Available online 20 October 2020

Table 1
Bulk (B) oxide composition obtained from XRF.

	SiO_2	Al_2O_3	CaO	Fe_2O_3	MgO	SO_3	Na_2O	K_2O	Other
Ash 1 (B)	21.23	13.99	28.35	5.53	6.79	4.88	1.92	0.46	16.84
Ash 2 (B)	28.08	14.40	26.55	4.54	3.67	11.56	1.40	0.52	9.28
Ash 3 (B)	41.25	16.40	20.68	6.79	4.10	0.99	4.27	0.42	5.11
Ash 4 (B)	39.62	16.58	20.92	6.15	4.27	4.09	2.37	0.45	5.55
Ash 5 (B)	36.99	18.83	23.83	6.21	5.10	1.13	1.68	0.58	5.66
Ash 6 (B)	56.51	19.85	10.16	5.81	2.94	0.34	0.63	1.35	2.41
Ash 7 (B)	38.21	19.37	21.54	6.20	5.19	1.28	1.60	0.63	5.98
Ash 8 (B)	49.82	23.84	13.30	4.41	3.27	0.70	0.91	0.54	3.21
Ash 9 (B)	52.42	19.59	14.14	4.78	3.17	0.86	0.78	1.07	3.17
Ash 10 (B)	38.88	18.03	23.53	5.97	4.98	0.91	1.53	0.58	5.58
Ash 11 (B)	35.63	19.18	14.59	4.98	3.38	2.67	7.64	0.71	11.22
Ash 12 (B)	37.26	22.43	21.26	5.44	4.07	0.95	1.50	0.56	6.54
Ash 13 (B)	32.79	16.34	27.76	5.79	6.87	1.82	1.66	0.39	6.59
Ash 14 (B)	52.28	22.93	3.22	13.04	0.99	0.85	0.92	2.58	3.19
Ash 15 (B)	37.57	19.08	22.39	5.57	5.48	0.85	1.78	0.46	6.84
Ash 16 (B)	59.62	23.97	1.31	6.56	1.16	0.35	1.31	1.07	4.65

Table 2
Mineralogy of the fly ashes and total glass content as determined by QXRD (weight %). The n.d. indicator indicates not detected. Mayenite may include wadalite, and ettringite may include thaumasite. Trace (t) amounts treated as n.d. for calculations.

	Ash 1	Ash 2	Ash 3	Ash 4	Ash 5	Ash 6	Ash 7	Ash 8	Ash 9	Ash 10	Ash 11	Ash 12	Ash 13	Ash 14	Ash 15	Ash 16
Quartz	1.4	3.5	8.1	9.3	10.1	22.7	7.0	14.2	12.9	10.5	3.0	8.4	11.2	9.0	13.9	17.2
Wadalite	4.1	n.d.	n.d.	n.d.	n.d.	n.d.	n.d.	n.d.	n.d.	n.d.	n.d.	n.d.	n.d.	n.d.	n.d.	n.d.
Augite	n.d.	n.d.	14.8	10.8	n.d.	n.d.	n.d.	n.d.	n.d.	n.d.	n.d.	n.d.	n.d.	n.d.	n.d.	n.d.
Akermanite	n.d.	n.d.	10.4	13.5	1.7	n.d.	1.4	n.d.	n.d.	1.8	2.0	n.d.	1.9	n.d.	1.8	n.d.
Anorthite	n.d.	n.d.	11.9	1.7	n.d.	n.d.	n.d.	n.d.	0.7	n.d.	n.d.	n.d.	n.d.	n.d.	n.d.	n.d.
Merwinite	n.d.	n.d.	n.d.	6.5	10.0	n.d.	5.8	2.2	2.0	11.3	2.7	4.2	14.2	n.d.	10.6	n.d.
Periclase	1.2	1.5	1.0	1.0	2.7	0.3	2.0	1.3	0.6	3.2	1.0	1.4	6.5	n.d.	4.0	n.d.
Mayenite	n.d.	5.0	n.d.	n.d.	n.d.	n.d.	n.d.	n.d.	n.d.	n.d.	n.d.	n.d.	n.d.	n.d.	n.d.	n.d.
Lime	0.5	n.d.	n.d.	n.d.	0.8	n.d.	n.d.	0.3	n.d.	0.6	n.d.	0.4	2.4	n.d.	0.9	n.d.
Anhydrite	8.3	n.d.	n.d.	0.8	1.8	0.7	1.8	1.0	1.0	0.9	0.5	1.2	2.3	1.3	1.1	n.d.
Hannebachite	n.d.	10.0	n.d.	n.d.	n.d.	n.d.	n.d.	n.d.	n.d.	n.d.	n.d.	n.d.	n.d.	n.d.	n.d.	n.d.
Ettringite	n.d.	2.0	t	n.d.	n.d.	n.d.	n.d.	n.d.	n.d.	n.d.	n.d.	n.d.	n.d.	n.d.	n.d.	n.d.
Mullite	n.d.	n.d.	n.d.	n.d.	5.2	8.9	t	18.4	5.9	4.4	t	5.2	3.9	13.9	7.0	16.1
Haturite	n.d.	n.d.	n.d.	n.d.	n.d.	n.d.	n.d.	n.d.	n.d.	n.d.	n.d.	n.d.	n.d.	n.d.	n.d.	n.d.
Larnite	n.d.	n.d.	n.d.	n.d.	n.d.	n.d.	n.d.	n.d.	n.d.	n.d.	n.d.	n.d.	n.d.	n.d.	n.d.	n.d.
Brownmillerite	n.d.	n.d.	n.d.	n.d.	T	n.d.	n.d.	n.d.	n.d.	2.1	n.d.	n.d.	n.d.	n.d.	1.6	n.d.
Thenardite	n.d.	n.d.	n.d.	n.d.	n.d.	n.d.	n.d.	n.d.	n.d.	n.d.	4.0	n.d.	n.d.	n.d.	n.d.	n.d.
Hematite	n.d.	n.d.	n.d.	n.d.	1.5	0.4	1.0	0.5	0.3	0.5	0.5	0.5	1.0	1.3	1.3	0.8
Magnetite	n.d.	n.d.	n.d.	n.d.	n.d.	0.5	n.d.	n.d.	n.d.	n.d.	n.d.	n.d.	n.d.	3.0	n.d.	0.7
Total glass %	84.5	78.0	53.8	56.4	66.1	66.5	81.0	62.1	76.6	64.7	86.3	78.7	56.2	71.5	57.8	65.2

Table 3
Oxide composition (weight %) of the crystalline components from Ref. [25].

	SiO_2	Al_2O_3	CaO	Fe_2O_3	MgO	SO_3	Na_2O	K_2O	Other
Quartz	100	–	–	–	–	–	–	–	–
Wadalite	20.39	21.15	42.3	3.01	3.04	–	–	–	1.11
Augite	48.30	8.63	21.35	6.08	14.35	–	1.31	–	–
Akermanite	44.08	–	41.44	–	14.78	–	–	–	–
Anorthite	44.40	35.84	19.2	–	–	–	0.506	–	–
Merwinite	36.56	–	51.18	–	12.26	–	–	–	–
Periclase	–	–	–	–	100	–	–	–	–
Mayenite	–	51.47	48.53	–	–	–	–	–	–
Lime	–	–	100	–	–	–	–	–	–
Anhydrite	–	–	41.19	–	–	58.81	–	–	–
Hannebachite	–	–	43.42	–	–	49.61	–	–	7.00
Ettringite	–	8.12	26.81	–	–	19.14	–	–	46.00
Mullite	28.21	71.79	–	–	–	–	–	–	–
Haturite	–	–	73.68	–	–	26.32	–	–	–
Larnite	36.56	–	51.18	–	12.26	–	–	–	–
Brownmillerite	–	–	–	–	100	–	–	–	–
Thenardite	–	–	–	–	–	56.37	43.63	–	–
Hematite	–	–	–	100	–	–	–	–	–
Magnetite	–	–	–	100	–	–	–	–	–

calcium hydroxide content and capillary porosity [4].

The structural composition of the fly ash influences the reactivity, particularly the fraction of each specific oxide that is glassy versus crystalline [1,3,9]. As a result, the bulk chemical composition of fly ash is insufficient to predict the reactivity of fly ash [6,7]. Prior work has demonstrated that typically the glassy (also referred to as amorphous or

Table 4
Chemical composition of the OPC used in this study as determined by XRF, rounded to two significant digits.

	Na_2O	MgO	Al_2O_3	SiO_2	SO_3	K_2O	CaO	Fe_2O_3
Mass %	0.17	3.20	3.62	20.90	2.13	0.53	61.63	3.20

vitreous) phases of fly ash are reactive in cementitious systems. At the same time, the crystalline components are typically not reactive [11,12]. For equilibrium speciation in cement/fly ash systems to be modeled appropriately, an accurate characterization of the glass phases in fly ash is needed. Furthermore, the actual reactivity of different fly ashes can be quite variable, generally ranging from 20% to 60% [7].

Despite the general knowledge that the reactivity of fly ash and other SCMs is limited, many historical modeling studies have used the bulk composition as an input for thermodynamic calculations [13–16]. The use of SCM bulk composition as a model input, when there is evidence that this is not entirely correct, appears to be due to the absence of an established means to determine the reactivity of materials other than OPC. Some have modeled SCM by only allowing a portion of the SCM to react; however, this is relatively arbitrary [17]. Recent works on synthetic fly ash glass [9] and fly ash [11] have elucidated the role of individual glass structure on the overall fly ash reactivity.

Several experimental methods to estimate the overall degree of reaction (DoR*) of the fly ash have been proposed [7,18–21]. However, many of these approaches often require extensive examination using sophisticated experimental techniques. As a result, they are not frequently used in practice. A recently proposed DoR* test, which is also

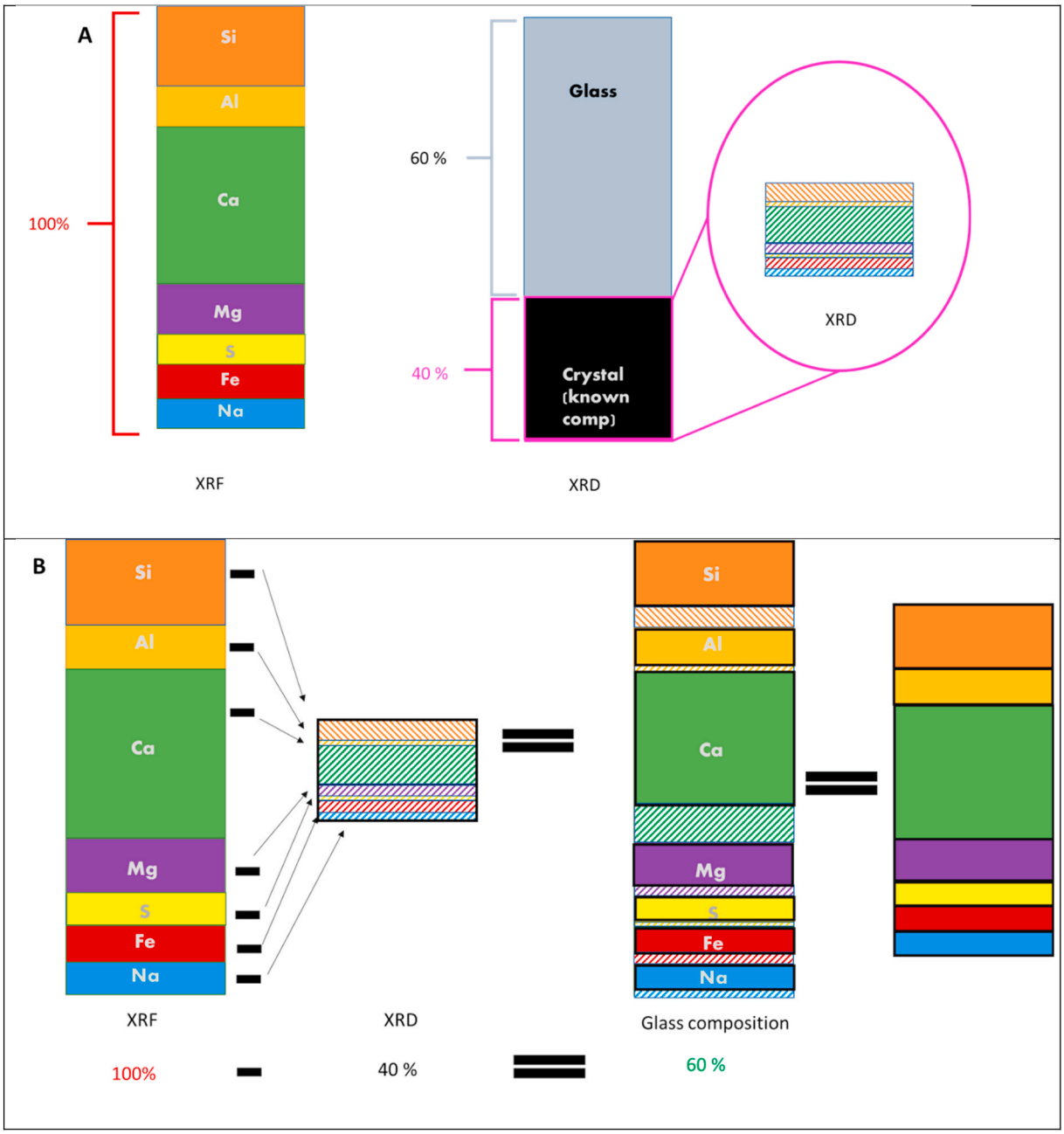

Fig. 1. A) Conceptual representation of the bulk content as measured by XRF and the overall glass and individual crystal content as measured by QXRD, and B) conceptual representation of the determination of glass content as accomplished through subtracting the individual crystal phases in QXRD from XRF. Other oxides may be present in the ashes, but for clarity are not shown in this conceptual figure.

Table 5
Bulk (B) fly ash composition obtained from XRF, DoR*, and glass (DoR_{ph}*) composition of the fly ash oxides in weight % of ash, excluding LOI.

	SiO_2	Al_2O_3	CaO	Fe_2O_3	MgO	SO_3	Na_2O	K_2O	Other
Ash 1 (B)	21.23	13.99	28.35	5.53	6.79	4.88	1.92	0.46	16.84
Ash 1 (DoR*)	8.07	5.32	10.77	2.10	2.58	1.86	0.73	0.17	6.40
Ash 1 (DoR_{ph}*)	19.00	13.13	22.70	5.41	5.47	0.00	1.92	0.46	16.71
Ash 2 (B)	28.08	14.40	26.55	4.54	3.67	11.56	1.40	0.52	9.28
Ash 2 (DoR*)	24.58	11.66	19.24	4.54	2.17	6.22	1.40	0.52	8.96
Ash 2 (DoR_{ph}*)	12.64	6.48	11.95	2.04	1.65	5.20	0.63	0.24	4.17
Ash 3 (B)	41.25	16.40	20.68	6.79	4.10	0.99	4.27	0.42	5.11
Ash 3 (DoR*)	16.14	10.86	10.95	5.89	0.00	0.99	4.01	0.42	4.38
Ash 3 (DoR_{ph}*)	9.49	3.77	4.76	1.56	0.94	0.23	0.98	0.10	1.17
Ash 4 (B)	39.62	16.58	20.92	6.15	4.27	4.09	2.37	0.45	5.55
Ash 4 (DoR*)	16.02	15.04	9.07	5.49	0.00	3.62	2.21	0.45	4.72
Ash 4 (DoR_{ph}*)	7.92	3.32	4.18	1.23	0.85	0.82	0.47	0.09	1.11
Ash 5 (B)	36.99	18.83	23.83	6.21	5.10	1.13	1.68	0.58	5.66
Ash 5 (DoR*)	20.98	15.09	16.42	4.71	0.91	0.07	1.68	0.58	5.66
Ash 5 (DoR_{ph}*)	11.10	5.65	7.15	1.86	1.53	0.34	0.50	0.17	1.70
Ash 6 (B)	56.51	19.85	10.16	5.81	2.94	0.34	0.63	1.35	2.41
Ash 6 (DoR*)	31.30	13.46	9.87	4.91	2.64	−0.07	0.63	1.35	2.41
Ash 6 (DoR_{ph}*)	25.99	9.13	4.67	2.67	1.35	0.16	0.29	0.62	1.11
Ash 7 (B)	38.21	19.37	21.54	6.20	5.19	1.28	1.60	0.63	5.98
Ash 7 (DoR*)	28.47	19.37	17.25	6.10	2.27	0.22	1.60	0.63	5.98
Ash 7 (DoR_{ph}*)	14.90	7.55	8.40	2.42	2.02	0.50	0.62	0.25	2.33
Ash 8 (B)	49.82	23.84	13.30	4.41	3.27	0.70	0.91	0.54	3.21
Ash 8 (DoR*)	29.62	10.64	11.47	3.91	1.70	0.11	0.91	0.54	3.21
Ash 8 (DoR_{ph}*)	20.92	10.01	5.59	1.85	1.37	0.29	0.38	0.23	1.35
Ash 9 (B)	52.42	19.59	14.14	4.78	3.17	0.86	0.78	1.07	3.17
Ash 9 (DoR*)	36.82	15.36	12.42	4.48	2.22	0.27	0.78	1.07	3.17
Ash 9 (DoR_{ph}*)	20.97	7.84	5.66	1.91	1.27	0.34	0.31	0.43	1.27
Ash 10 (B)	38.88	18.03	23.53	5.97	4.98	0.91	1.53	0.58	5.58
Ash 10 (DoR*)	22.21	14.87	16.03	5.47	0.00	0.38	1.53	0.58	5.58
Ash 10 (DoR_{ph}*)	14.77	6.85	8.94	2.27	1.89	0.35	0.58	0.22	2.12
Ash 11 (B)	35.63	19.18	14.59	4.98	3.38	2.67	7.64	0.71	11.22
Ash 11 (DoR*)	30.76	18.86	11.10	4.48	1.75	1.61	7.64	0.71	9.38
Ash 11 (DoR_{ph}*)	13.90	7.48	5.69	1.94	1.32	1.04	2.98	0.28	4.38
Ash 12 (B)	37.26	22.43	21.26	5.44	4.07	0.95	1.50	0.56	6.54
Ash 12 (DoR*)	25.85	18.70	18.21	4.94	2.16	0.24	1.50	0.56	6.54
Ash 12 (DoR_{ph}*)	17.14	10.32	9.78	2.50	1.87	0.44	0.69	0.26	3.01
Ash 13 (B)	32.79	16.34	27.76	5.79	6.87	1.82	1.66	0.39	6.59
Ash 13 (DoR*)	14.06	13.54	16.36	4.79	0.00	0.46	1.66	0.39	6.59
Ash 13 (DoR_{ph}*)	9.51	4.74	8.05	1.68	1.99	0.53	0.48	0.11	1.91
Ash 14 (B)	52.28	22.93	3.22	13.04	0.99	0.85	0.92	2.58	3.19
Ash 14 (DoR*)	39.36	12.95	2.69	8.74	0.99	0.08	0.92	2.58	3.19
Ash 14 (DoR_{ph}*)	25.09	11.01	1.55	6.26	0.48	0.41	0.44	1.24	1.53
Ash 15 (B)	37.57	19.08	22.39	5.57	5.48	0.85	1.78	0.46	6.84
Ash 15 (DoR*)	17.03	14.05	14.88	4.27	0.00	0.20	1.78	0.46	6.84
Ash 15 (DoR_{ph}*)	13.90	7.06	8.29	2.06	2.03	0.31	0.66	0.17	2.53
Ash 16 (B)	59.62	23.97	1.31	6.56	1.16	0.35	1.31	1.07	4.65
Ash 16 (DoR*)	37.88	12.42	1.31	5.06	1.16	0.35	1.31	1.07	4.65
Ash 16 (DoR_{ph}*)	22.66	9.11	0.50	2.49	0.44	0.13	0.50	0.41	1.77

Table 6
Groupings of study fly ashes based on glass content.

	Group 1	Group 2	Group 3	Group 4
Glass content (%)	54–58	62–66	72–78	78–85
Glass content (Qualitative)	Low	Low-Moderate	Moderate-High	High

used in this paper, determines the reactive fraction of fly ash by measuring the heat release (Q) and the calcium hydroxide (CH) consumption and the DoR* when fly ash is reacted with calcium hydroxide in a pore solution at high temperature and pH [19]. The results of this test, Q and CH consumption, are superimposed on plots of predetermined degrees of reaction of pure SiO_2 and Al_2O_3 systems to estimate a value of DoR* for fly ash. The inputs for thermodynamic modeling are determined for each bulk oxide phase of the fly ash by multiplying the bulk composition by DoR*. The determination of DoR* using this approach is relativity inexpensive, straightforward, and reasonably accurate for most fly ashes [7]; however, it requires the determination of heat release and CH consumption, which may not be not possible in all laboratories.

2. Research objective

The objective of this paper is two-fold: First, the paper presents a method for determining the reactive (glass) fraction of fly ash to be used in thermodynamic calculations. In this method, the fraction of crystalline oxides (measured using quantitative x-ray diffraction, QXRD) is subtracted from the bulk oxide content (measured using x-ray fluorescence, XRF) to establish a DoR for each phase (DoR_{ph}*). This DoR_{ph}* is used to determine the reactive amount of each phase of the fly ash to be used as an input for thermodynamic calculations. Second, this paper demonstrates the improved predictive ability of the thermodynamic models by incorporating fly ash reactivity as a model input. Three different methods for obtaining fly ash DoR inputs for thermodynamic models are compared.

3. Materials and methods

The following sections first describe the details of the experimental procedures used in this study, as well as the thermodynamic modeling approaches. Following these detailed descriptions are sections explaining how these tools were used to perform the modeling in this paper.

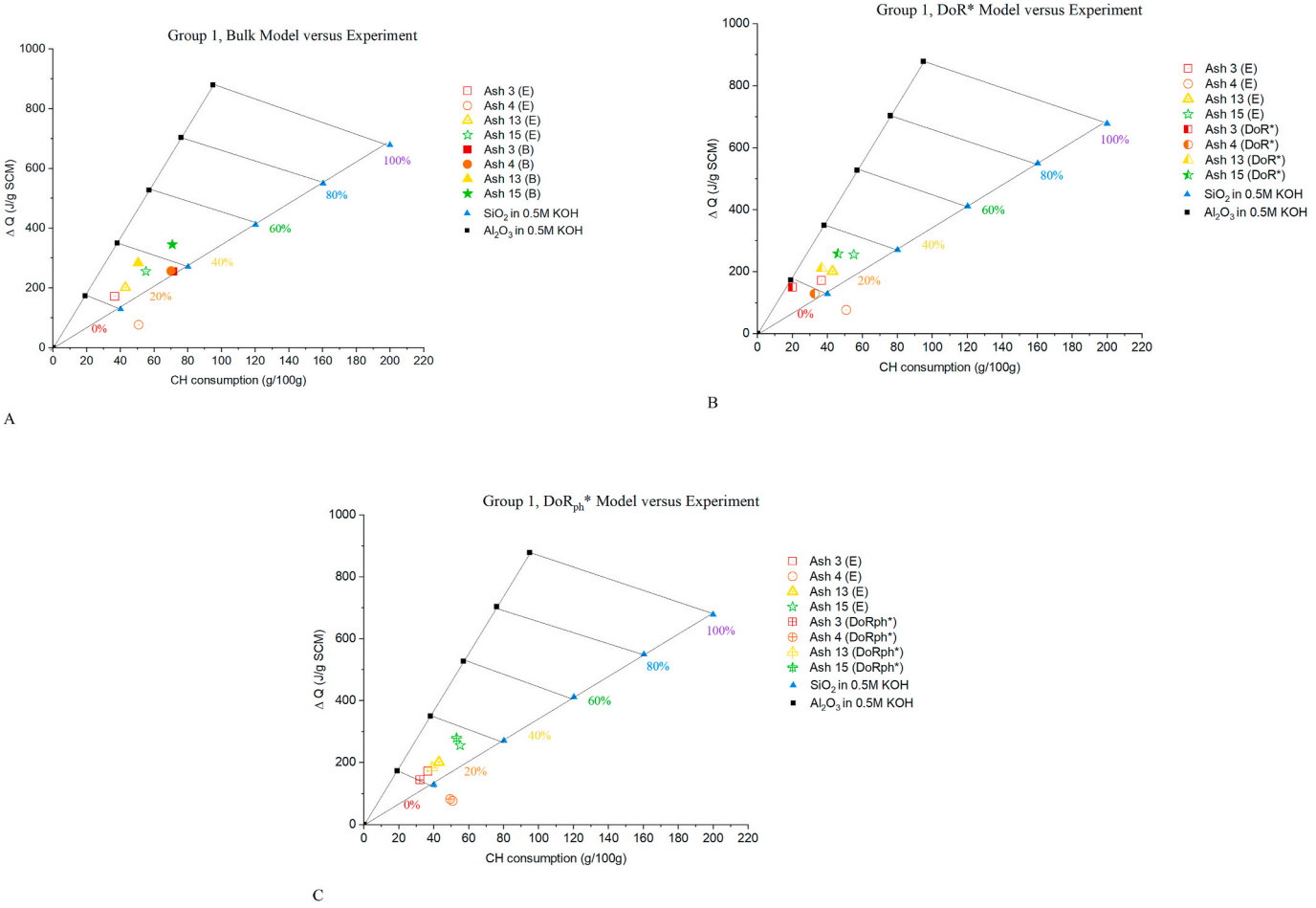

Fig. 2. Comparison of experimental measurements of CH consumption and heat release to A) bulk thermodynamic model, B) DoR* thermodynamic model, and C) DoR_{ph}* thermodynamic model for Group 1 (low glass content) fly ashes.

3.1. Experimental methods

3.1.1. Determination of bulk, crystalline, and glass content of fly ash

XRF was used in this study to measure the bulk composition of the fly ashes and cement. Before each XRF analysis, a calibration was performed with known standards to quantify the elements studied accurately [22]. Details of the XRF testing using the fused bead procedure and analysis are provided in Ref. [22–24]. Table 1 shows the results of the bulk XRF analysis.

QXRD analysis was performed to obtain the crystalline composition of the fly ashes. Corundum was used as an internal reference standard to estimate the amorphous content. The X-ray diffraction analysis was performed on a Panalytical X'Pert Pro diffractometer, equipped with a Cu X-ray source and an X'celerator detector, operating at the following X-ray conditions: voltage: 40 kV; current: 40 mA; range: 5–70 deg 2θ; step size: 0.017 deg 2θ; time per step: 30 s; divergence slit: fixed, angle 0.5°. The crystalline mineral phases were identified in X'Pert HighScore Plus using the PDF-4 Minerals ICDD database. The quantities of the crystalline minerals were determined using the Rietveld method. The Rietveld method is based on the calculation of the full diffraction pattern from crystal structure data. The amounts of the crystalline minerals were recalculated based on a known percent of corundum, and the remainder to 100% was considered X-ray amorphous material. Details of the Rietveld method can be found in the literature [7,26,27]. The results of the QXRD analysis are shown in Table 2. The oxide composition of each mineral identified by QXRD is taken from Ref. [25] and shown in Table 3.

3.1.2. The DoR* test

The DoR* of the fly ashes (i.e., the maximum overall reactive fraction of each fly ash) was measured in accordance with the method proposed in Ref. [7,19]. The test is based on mixing reagent grade calcium hydroxide (CH) and fly ash in a 3:1 mass ratio in a 0.5 M potassium hydroxide (KOH) solution at 50 °C. Isothermal calorimetry (IC) and thermogravimetric analysis (TGA) are used to measure heat release (Q) for ten days and CH consumption at ten days, respectively. Measured heat release and CH consumption are plotted against thermodynamically calculated reference lines for Al_2O_3 and SiO_2 in 0.5 M KOH solution at degrees of reaction from 0% to 100%. Thermodynamic reference lines were computed using the GEMS geochemical code, and Cemdata v.18.01 database [2] for each reference line by entering the bulk solution composition at each DoR* step and calculating the free enthalpy of reaction and the consumption of CH. These reference lines provide the theoretical values for the expected heat released, and CH consumed in hydraulic and pozzolanic reactions. The DoR* of the fly ash, as measured by TGA and isothermal calorimetry, can be read in reference to these lines.

3.1.3. Determination of OPC and paste properties

The chemical composition of the OPC was determined by XRF analysis (Table 4). The CH content of pastes containing Ash 4 and OPC at fly ash replacement levels (by mass) of 0%, 20%, and 40% and w/b of 0.35, 0.45, and 0.55 were measured at 56-days using thermogravimetric analysis. Each analysis was performed three times, and the mean and standard deviations are reported. Details of the XRF and TGA methods can be found in Ref. [7,22–24]. The 56-day test was chosen for

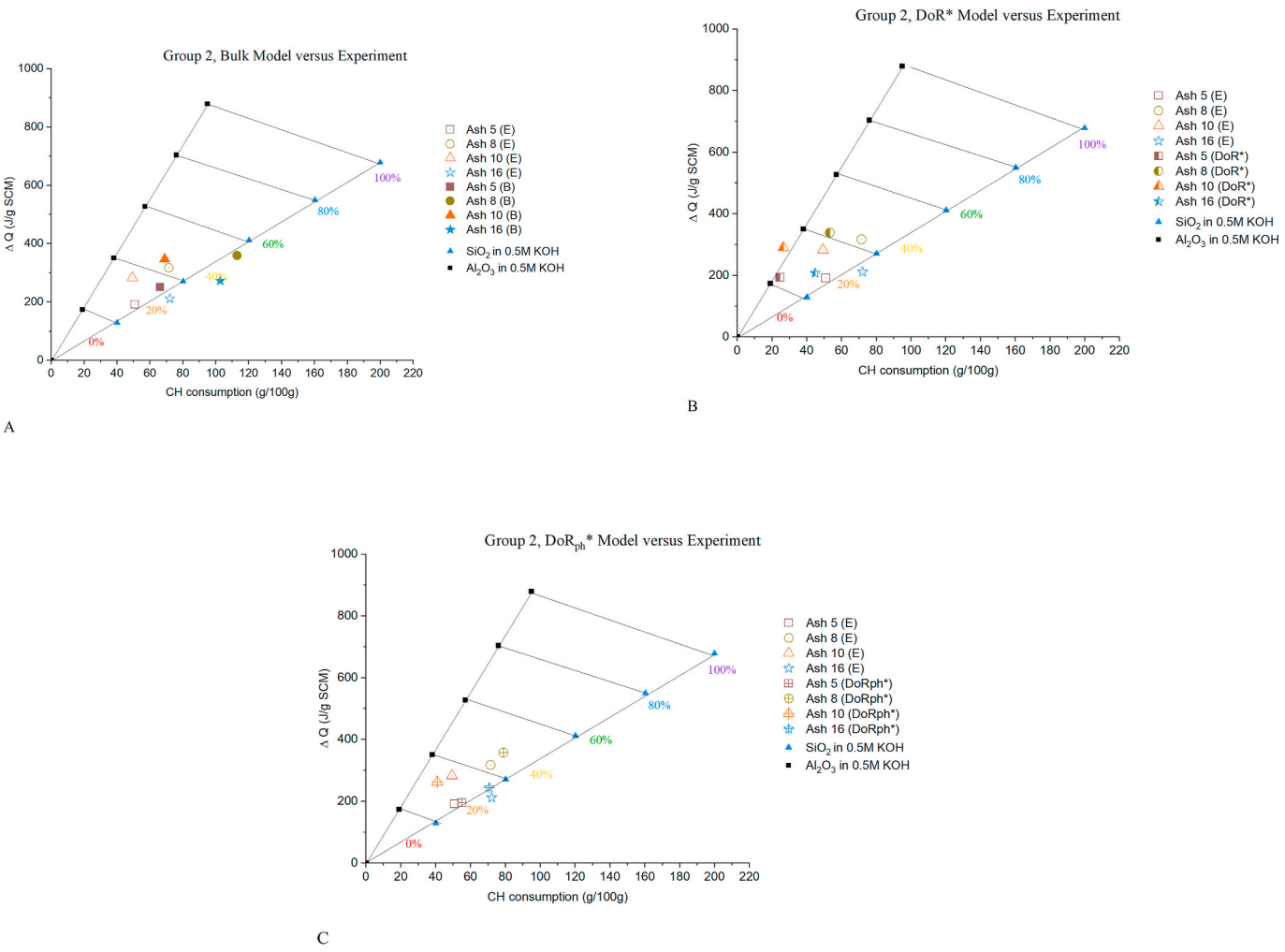

Fig. 3. Comparison of experimental measurements of CH consumption and heat release to A) bulk thermodynamic model, B) DoR* thermodynamic model, and C) DoR_{ph}* thermodynamic model for Group 2 (low-moderate glass content) fly ashes.

experimental and modeling purposes since the 56-day time frame accounts for nearly full system hydration, and the primary purpose of this study is to understand the maximum reactable fraction of fly ashes at equilibrium conditions. The 56-day age is late enough to not be appreciably influenced by early age kinetics, while allowing for the reactable fraction of the fly ashes to be tested at an age that many agencies use for acceptance.

3.2. Determination of the reactive fly ash phase quantity input for thermodynamic calculations

3.2.1. Using bulk fly ash composition

In this approach, the reactive and non-reactive phases of fly ash are not differentiated, and only the bulk composition of the fly ash is provided as input to thermodynamic calculations.

*3.2.2. Calculation of reactive fly ash phases using DoR**

In this approach, the overall reactivity of the fly ash (DoR*) is determined by the reactivity test [7] and the inputs for thermodynamic modeling are determined for each bulk oxide phase of the fly ash by multiplying the bulk composition by DoR*.

3.2.3. Calculation of reactive fly ash phases using glass content of each phase (DoR_{ph})*

This section describes the method for determining the reactive (glass) fraction of fly ash that is used to calculate the reactive fly ash phases that are the input in thermodynamic calculations. Conceptually, this method subtracts the measured fraction of crystalline oxides (measured using quantitative x-ray diffraction (QXRD)) from the bulk oxide content (determined using x-ray fluorescence (XRF)) to establish a DoR for each phase (DoR_{ph}*) as shown in Fig. 1. The DoR_{ph}* is computed using Equation (1):

$$DoR^{*}_{ph} = DoR_{ph,B} - \sum DoR_{ph,C} \quad (1)$$

where $DoR_{ph,B}$ is the bulk content of each phase (g oxide/g of fly ash) as measured by XRF, $DoR_{ph,C}$ is the sum of each crystalline oxide as measured by QXRD (g oxide/g fly ash), and DoR_{ph}* is the glassy (reactive) fraction of each phase (g oxide/g fly ash). The units of DoR_{ph}* are computed as a fraction (i.e., the percent of each phase (i.e., oxide) that is glassy or reactive).

Equation (2) shows an example of the DoR_{ph}* calculation for SiO_2 for a hypothetical fly ash containing only two siliceous minerals, quartz (quartz = 100% SiO_2) and mullite (mullite = 28.21% SiO_2). The measured bulk SiO_2 content of the hypothetical fly ash is 60%, and the measured QXRD abundance for the hypothetical fly ash are 15% quartz and 5% mullite:

$$DoR^{*}_{SiO2} = 0.60 - [(1 \times 0.15) + (0.2821 \times 0.05)] = 0.43 \quad (2)$$

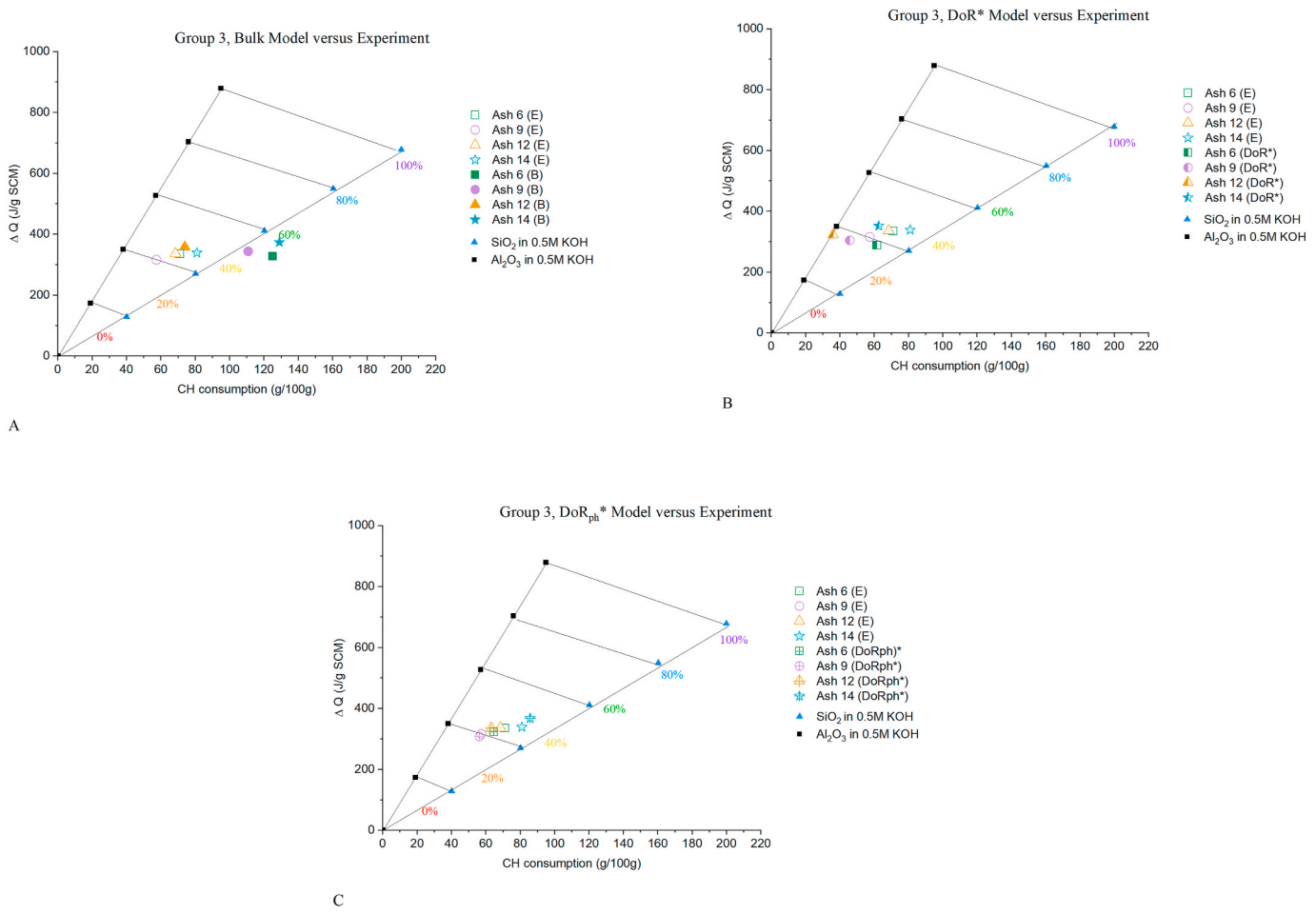

Fig. 4. Comparison of experimental measurements of CH consumption and heat release to A) bulk thermodynamic model, B) DoR* thermodynamic model, and C) DoR_{ph}* thermodynamic model for Group 3 (moderate-high glass content) fly ashes.

3.3. Thermodynamic calculations

Hydrated phase assemblages of fly ash and pastes were computed using the GEMS3K geochemical code [28–30]. Thermodynamic data were obtained from the Cemdata v.18.01 [2] database. GEMS3K computes equilibrium phase assemblages and speciation based on the total chemical composition of the system. GEMS simulations are based on a Gibbs Free Energy Minimization algorithm. Therefore, reactions proceed to theoretically infinite time, or the time when the free energy of the system is minimized [28].

Free enthalpy of the reactions was calculated using data from the internally consistent Cemdata v.18.01 database (Equation (3)).

$$\Delta H_{reaction} = \sum n_p \Delta H_{f\ (products)} - \sum n_r \Delta H_{f\ (reactants)} \quad (3)$$

where ΔH is the standard enthalpy of formation (Joules), n_p is the number of moles in the products of the reaction (moles), and n_r is the number of moles in the reactants.

Thermodynamic calculations to determine the heat of reaction (Q) and CH consumption were performed for each fly ash three times: First, using the bulk chemical composition of the ash (B), and second, using only the glassy phase composition (DoR_{ph}*) and finally using the overall fly ash DoR*. For the bulk modeling, the fly ash bulk composition, as reported in Table 1, is used as an input for the thermodynamic calculations. For the DoR_{ph}* modeling, the glass composition of each fly ash (referred to as DoR_{ph}*), as reported in the respective columns in Table 5, is used as an input for the thermodynamic calculations. Finally, in the DoR* thermodynamic models, the measured DoR* of the overall fly ash is used as an input for the thermodynamic calculations. Here, for each fly ash, each bulk oxide is multiplied by the same measured DoR* value. These values are also listed in Table 5.

Thermodynamic calculations were also performed on fly ash/OPC pastes at various w/b and fly ash mass replacement levels using the three modeling strategies. For all three modeling strategies, the kinetics of the reaction are modeled using the MPK model [26]; however, the MPK model inputs for the fly ash phases differ for the three strategies. The MPK model uses the maximum reactable fraction of each ash as in input, and applies a set of kinetic rules to predict the reacted fraction of the ash at each age. For the bulk model, the bulk content of the fly ash phases is used as an input. For the DoR* model, the DoR* of each primary fly ash phase is used as an input. For the DoR_{ph}* model, the DoR_{ph}* of each primary fly ash phase is used as the MPK model input.

4. Discussion of results and comparison of approaches

4.1. Fly ash input data to be used in thermodynamic calculations

Table 5 summarizes the bulk chemical (B) DoR test (DoR*) and the glassy phase (DoR_{ph}*) composition of the ashes. Fly ashes 1, 2, and 4 are "off-spec" North American fly ashes, which fail to meet the specifications of ASTM C618 based on their physical or chemical properties. Ash 3 is a bottom ash.

4.2. Heat release and CH consumption of fly ash

As a matter of clarity in discussing the results, the 16 fly ashes are

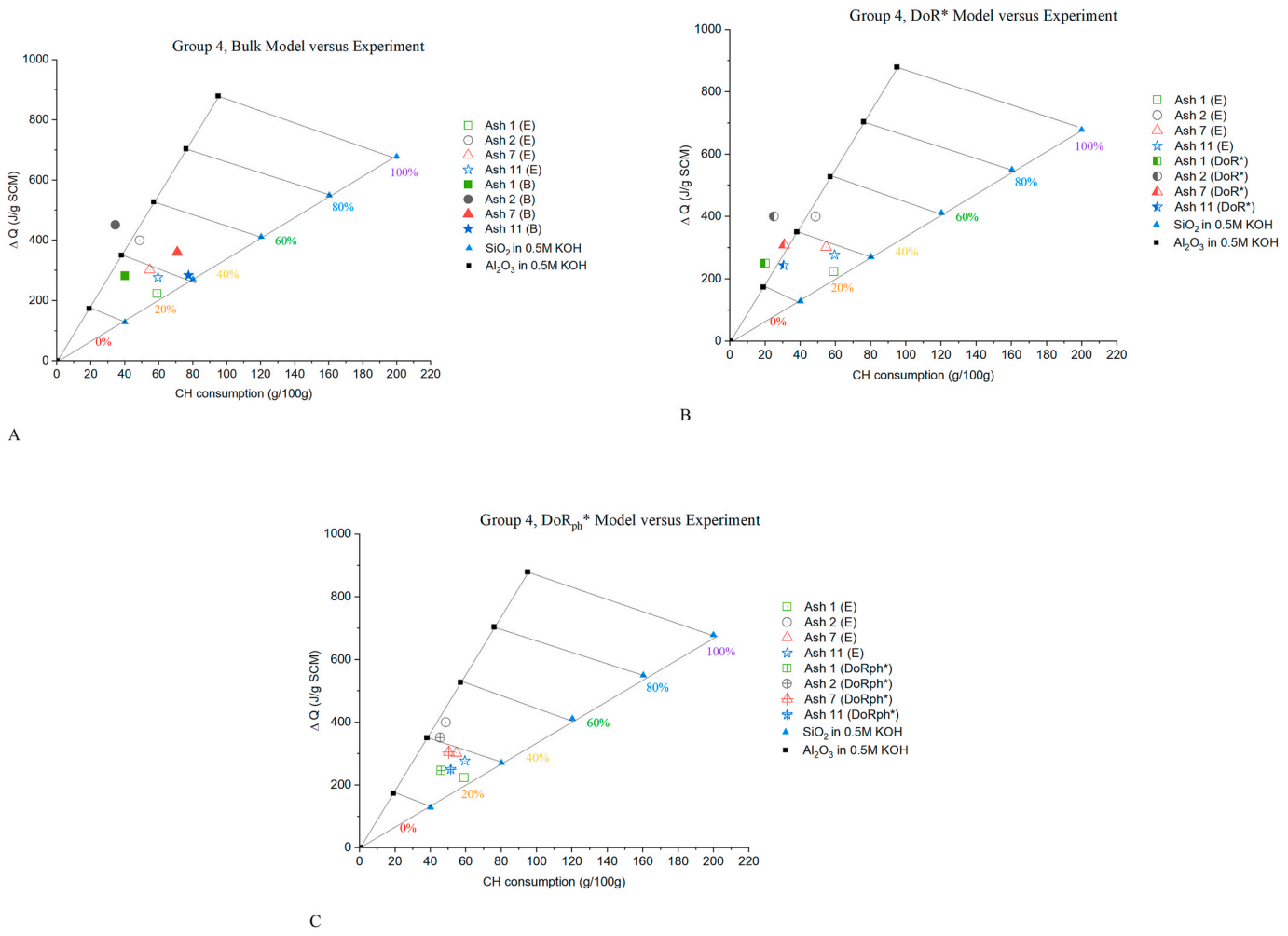

Fig. 5. Comparison of experimental measurements of CH consumption and heat release to A) bulk thermodynamic model, B) DoR* thermodynamic model, and C) DoR_{ph}* thermodynamic model for Group 4 (high glass content) fly ashes.

divided into four groups based on their measured glass percentages (Table 6). The binning of groups is based on the glass percentage in the distribution of the results for the 16 fly ashes.

The three fly ash thermodynamic modeling approaches (bulk, DoR* and DoR_{ph}*) are compared to the experimentally measured values for CH consumption and heat release. CH consumption, along with heat release, is the current state-of-the-art for determining the fly ash reactivity, and as such is used in this study to validate thermodynamic predictions. Figs. 2–5 provide results of the heat release versus CH consumption as a function of glass content (Fig. 2 - low glass content; Fig. 3 - low-moderate glass content; Fig. 4 - moderate-high glass content, and Fig. 5 - high glass content). The experimental results are represented as open shapes, the bulk thermodynamic model results are represented as filled shapes, the DoR* thermodynamic model results as half-filled shapes, and the DoR_{ph}* thermodynamic model results as shapes with an "x".

Several observations can be drawn from Figs. 2–5. In general, the lower the glass content of an ash, the lower the ashes plot on the figures for CH consumption and heat release. For example, values for the low-glass content ashes (Group 1, Fig. 2) are between 20% and 35%, the low-moderate ashes (Group 2, Fig. 3) are between 35% and 45%, and the moderate-high ashes (Group 3, Fig. 4) are between 40% and 50%. However, the high-glass content ashes (Group 4, Fig. 5) deviate from this trend with the CH consumption and heat release falling between 35% and 50%. This deviation is likely related to the relatively low silica glass content in these ashes (Table 5), particularly for ash 1 (silica glass content of 19%), which plots just above the 35% line. The reactive silica in the ash contributes to its pozzolanicity (high reactive Si → high pozzolanicity). As a result, even when the ash has a relatively high total glass fraction, the relatively lower values of reactive silica (ash 1) tend to reduce the overall reactivity.

The next observation from Figs. 2–5 relates to the ability of the three modeling approaches to predict the measured CH consumption and heat release values. In all four groups of ashes, the bulk thermodynamic models are the least accurate predictors of these values, and the DoR_{ph}* models are the best predictors of these values. The DoR* models tend to provide reasonably good predictions of CH consumption and heat release, although the CH consumption may be underpredicted by the DoR* model. Therefore, it can be stated that the calculation of the reactive phases of fly ash using QXRD and XRF data (i.e., DoR_{ph}* approach) may serve as a potential alternative to the current calorimetric methods to calculate pozzolanic reactivity.

Finally, an important observation to draw from these results is that irrespective of bulk calcium content of the ashes, the glass fraction of calcium and other oxides appears to be fully reactive, and the crystalline fraction inert. This is in contrast to prior studies which suggest that for high calcium ashes, crystalline phases may be reactive. Further studies on potential reactivity of crystalline phases in high calcium ashes are warranted.

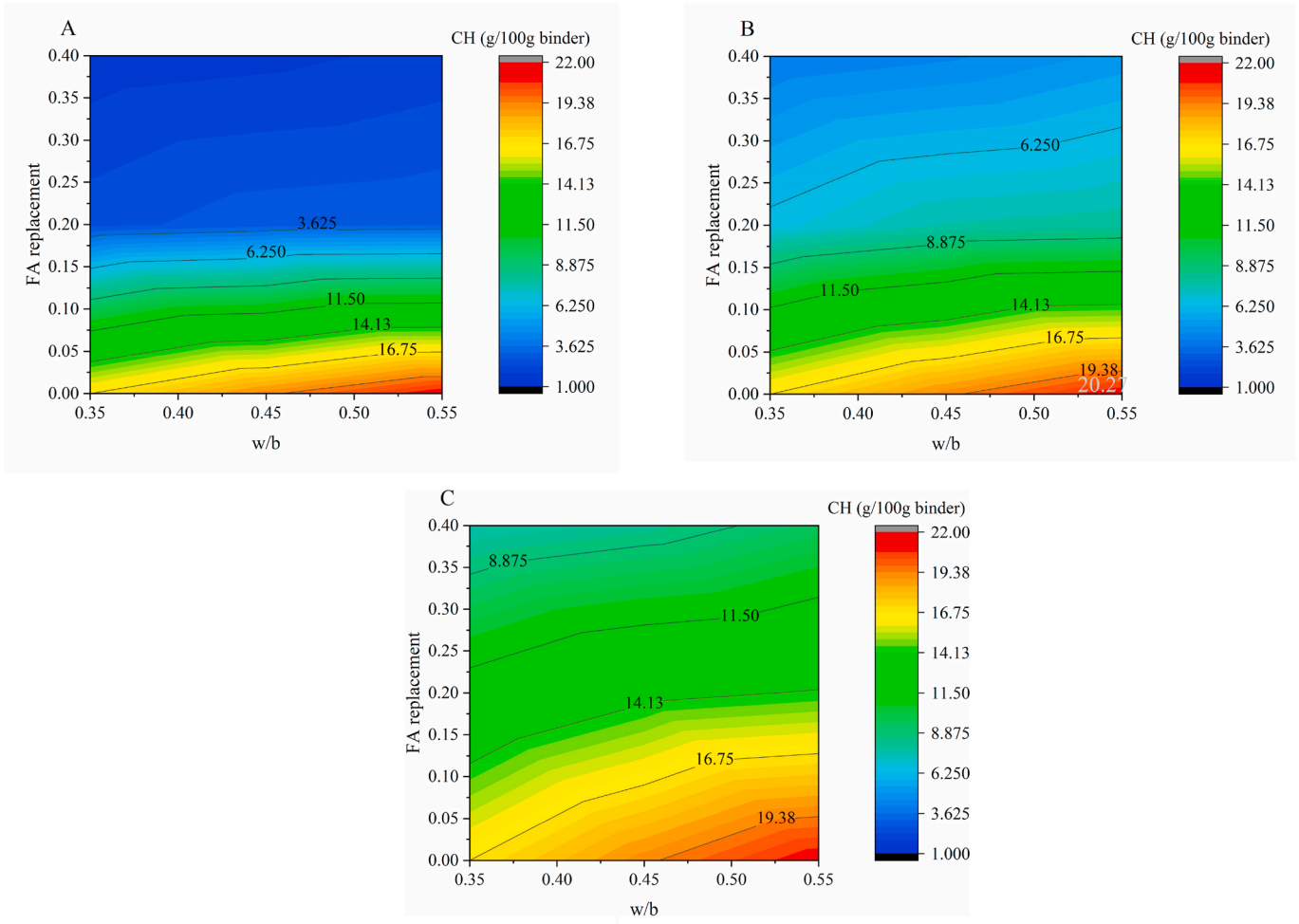

Fig. 6. Thermodynamic model results for CH content of pastes containing Ash 4 modeled at 56 days using the ash four bulk content (A), DoR* (B), and DoR_{ph}* (C) as inputs.

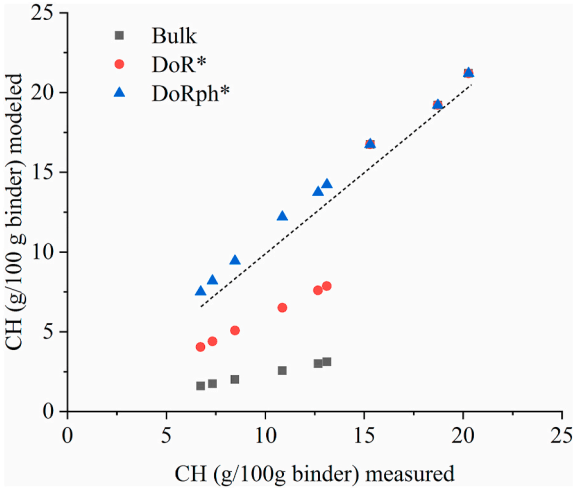

Fig. 7. Comparison of the CH content (g CH/100 g binder) of cement pastes at 56 days using Ash 4 at 0, 20, and 40% replacement levels for w/cm of 0.35, 0.45, 0.55. A 1:1 correlation line is also shown in the figure.

4.3. Thermodynamic modeling of cement pastes containing fly ash: comparing methods of modeling fly ash reactivity

Fig. 6 shows the calculated calcium hydroxide (CH) content in cement paste using thermodynamic modeling with the three approaches for determining the reactivity inputs (bulk (Fig. 6a), DoR* (Fig. 6b), DoR_{ph}* (Fig. 6c)). The pastes had a w/cm of 0.35, 0.45, and 0.55 with 0, 20, and 40% fly ash (Fly ash 4) replacement levels at 56 days. Contour lines represent the CH content.

Several observations can be drawn from Fig. 6. First, the model predictions for the OPC system (0% fly ash replacement) are the same for all simulations as expected since the input parameters for the fly ash are not used in the simulations. The models predict experimental values within 1.45 g CH/100 g binder for w/b 0.35, and <1 g CH/100 g binder for 0.45 and 0.55 w/b. This high level of accuracy is expected, as the MPK model used for simulating the chemical kinetics reduces to the Parrot-Killoh model for the OPC system, as demonstrated in multiple prior studies [3,29,30]. Second, for the systems containing fly ash, the approach based on the bulk properties predicts CH values that are approximately 75% less than the experimentally measured value. The thermodynamic model that uses the experimentally measured DoR* is approximately 35% less than the experimentally measured value, which is an improvement to the bulk composition approach. The thermodynamic model that uses the activity that was determined using the model presented in this paper (DoR_{ph}*) is approximately 10% higher than the experimentally measured value. For fly ashes with higher glass contents, the differences between the DoR* and DoR_{ph}* models are lower. Third, all three modeling strategies result in a reduction of the CH content with fly ash replacement level, as expected, due to the pozzolanic effect of fly ash, as well as by dilution. The bulk-paste models estimate more pozzolanic reaction than either of the other modeling strategies since

they assume all the fly ash is reacting. For fly ashes with higher glass contents, the differences between the DoR* and DoR_{ph}* models are smaller. These results also support the notion that the calculation of reactive fly ash phases using QXRD and XRF data (the DoR_{ph}* approach) may serve as a potential alternative to the current calorimetric methods for calculation of pozzolanic reactivity.

Fig. 7 shows a subset of the same data as Fig. 6: the CH content of the pastes modeled using the three thermodynamic approaches for all w/b and replacement levels, compared to the experimental measurements. A 1:1 correlation line on the figure is also shown. The purpose of Fig. 7 is to demonstrate how – for the datapoints where experimental data exist – the three thermodynamic approaches compare in terms of accuracy. It is evident that the bulk models underestimate CH, and that the DoR_{ph}* models most accurately predict CH content in the pastes. The DoR* models provide intermediate predictive ability.

In summary, the three thermodynamic modeling approaches have varying degrees of accuracy. The DoR_{ph}* approach is the most accurate for both fly ash and paste, while the bulk models are the least accurate.

5. Conclusions

Three approaches for thermodynamic modeling of fly ash reactivity in cementitious systems containing fly ash are presented. The three approaches are based on 1) bulk composition (bulk), 2) the degree of reactivity determined experimentally using the heat of hydration and calcium hydroxide consumption (DoR*), and 3) the degree of reactivity of fly ash at a phase level (DoR_{ph}*). The accuracy of thermodynamic models is improved in both the DoR* and DoR_{ph}* approaches as compared to approach based on bulk composition. The proposed method (DoR_{ph}*) is superior to the other methods. Fly ash with low glass content is the least reactive, and the reactivity increases with the overall glass content. The calculation of the reactive phases of fly ash using QXRD and XRF data (i.e., DoR_{ph}* approach) may serve as a potential alternative to the current calorimetric methods to calculate pozzolanic reactivity.

Declaration of competing interest

The authors declare that they have no known competing financial interests or personal relationships that could have appeared to influence the work reported in this paper.

Acknowledgments

The authors would like to acknowledge the financial support of the Electric Power Research Institute (EPRI) through grant 3002018795, ARPA-E through grant DE-AR0001143, and NSF CMMI 1728358. The authors also acknowledge Antara Choudhary for her laboratory assistance, particularly her measurement of the x-ray fluorescence (XRF) results. The authors thank Feyza Nur Sahan and Rita Ghantous for their laboratory measurements of calcium hydroxide used in Fig. 7.

References

[1] V. Jafari Azad, O.B. Isgor, Modeling chloride ingress in concrete with thermodynamically calculated chemical binding, Int. J. Adv. Eng. Sci. Appl. Math. 9 (No. 2) (2017) 97–108.
[2] B. Lothenbach, D. Kulik, T. Matschei, M. Balonis, Cemdata18: a chemical thermodynamic database for hydrated Portland cements and alkali-activated materials, Cement Concr. Res. 115 (2018) 476–502.
[3] V. Jafari Azad, P. Suraneni, O.B. Isgor, W.J. Weiss, Interpreting the pore structure of hydrating cement phases through a synergistic use of the Powers-Brownyard model, hydration kinetics, and thermodynamic calculations, Adv.Civil Eng. Mater. 6 (No. 1) (2017) 1–16.
[4] B. Lothenbach, A. Gruskovnjak, Hydration of alkali-activated slag: thermodynamic modelling, Adv. Cement Res. 19 (No. 2) (2007) 81–92.
[5] A. Abbas, G. Fathifazl, O.B. Isgor, A.G. Razaqpur, B. Fournier, S. Foo, Durability of recycled aggregate concrete designed with equivalent mortar volume method, Cement Concr. Compos. 31 (No. 8) (2009) 555–563.
[6] B. Lothenbach, E. Wieland, A thermodynamic approach to the hydration of sulphate-resisting Portland cement, Waste Manag. V. 26 (No. 7) (2006) 706–719.
[7] D. Glosser, A. Choudhary, O.B. Isgor, W.J. Weiss, Investigation of the reactivity of fly ash and its effect on mixture properties, ACI Mater. J. 116 (No. 4) (2019) 193–200.
[8] K. Aughenbaugh, P. Stutzman, M. Juenger, Identifying glass composition in fly ash, Front. Mater. 3 (No. 1) (2016) 1–10.
[9] P.T. Durdziński, R. Snellings, C. Dunant, M.B. Haha, K. Scrivener, Fly ash as an assemblage of model Ca–Mg–Na-aluminosilicate glasses, Cement Concr. Res. 78 (2015) 263–272.
[10] J. Ideker, O.B. Isgor, C. Li, V. Jafari, C. Verba, D.E. Rodriguez, Experimental and numerical modeling approach to elucidating damage mechanisms in cement-well casing-host rock settings for underground storage of CO_2, U.S. Department of Energy, National Energy Technology Laboratory, 2014. Report No. 8d29a40d-0c8e-43b4-b054-7c5323af37c4.
[11] R.T. Chancey, P.E. Stutzman, M. Juenger, Comprehensive phase characterization of crystalline and amorphous phases of a Class F fly ash, Cement Concr. Res. 40 (2010) 146–156.
[12] R. Snellings, Solution-controlled dissolution of supplementary cementitious material glasses at ph 13: the effect of solution composition on glass dissolution rates, J. Am. Ceram. Soc. 96 (No. 8) (2013) 2467–2475.
[13] M. Atkins, D.G. Bennet, A.C. Dawes, A thermodynamic model for blended cements, Cement Concr. Res. 22 (No. 2–3) (1992) 497–502.
[14] M. Atkins, F. Glasser, A. Kindness, Phase relation and solubility modelling in the $CaO–SiO_2–Al_2O_3–MgO–SO_3–H_2O$ system: for application to blended cements, Mater. Res. Soc. Symp. Proc. 212 (1991) 387–394.
[15] B. Lothenbach, K. Scrivener, R.D. Hooton, Supplementary cementitious materials, Cement Concr. Res. 41 (No. 12) (2011) 1244–1256.
[16] L. Chaignat, F. Winnefeld, B. Lothenbach, C. Muller, Beneficial use of limestone filler with calcium sulphoaluminate cement, Construct. Build. Mater. 26 (No. 1) (2012) 619–627.
[17] D. Glosser, V. Jafari Azad, P. Suraneni, B. Isgor, W.J. Weiss, Extension of Powers-Brownyard model to pastes containing supplementary cementitious materials, ACI Mater. J. 116 (No. 5) (2019) 205–216.
[18] R. Snellings, K.L. Scrivener, Rapid screening tests for supplementary cementitious materials: past and future, Mater. Struct. 49 (No. 8) (2016) 3265–3279.
[19] P. Suraneni, J. Weiss, Examining the pozzolanicity of supplementary cementitious materials using isothermal calorimetry and thermogravimetric analysis, Cement Concr. Compos. 83 (2017) 273–278.
[20] F. Puertas, A. Fernández-Jiménez, Mineralogical and microstructural characterisation of alkali-activated fly ash/slag pastes, Cement Concr. Compos. 25 (No. 3) (2003) 287–292.
[21] A. Matsuda, I. Maruyama, A. Meawad, S. Pareek, Y. Araki, Reaction, phases, and microstructure of fly ash-based alkali-activated materials, J. Adv. Concr. Technol. 17 (No. 3) (2019) 93–101.
[22] M.T. Chang, The Evaluation of Cementitious Pore Solution Composition and Electrical Resistivity Using X-Ray Fluorescence (XRF), M.S. Thesis, Oregon State University, 2017. Corvallis, OR.
[23] M.T. Chang, L. Montanari, P. Suraneni, W. Weiss, Expression of cementitious pore solution and the analysis of its chemical composition and resistivity using x-ray fluorescence, JoVE 139 (2018), e58432.
[24] M. Tsui Chang, P. Suraneni, L. Montanari, J.F. Muñoz, W.J. Weiss, Determination of chemical composition and electrical resistivity of expressed cementitious pore solutions using x-ray fluorescence, ACI Mater. J. 116 (No. 1) (2019) 155–164.
[25] D. Barthelmy, Minerology database. http://webmineral.com/. (Accessed 23 April 2020).
[26] D. Glosser, Equilibrium and Non-equilibrium Thermodynamic Modeling of Cement Pastes Containing SCM, Ph.D. Thesis, Oregon State University, 2020. Corvallis OR.
[27] K.L. Scrivener, T. Füllmann, E. Gallucci, G. Walenta, E. Bermejo, Quantitative study of Portland cement hydration by X-ray diffraction/Rietveld analysis and independent methods, Cement Concr. Res. 34 (No. 9) (2004) 1541–1547.
[28] D.A. Kulik, T. Wagner, S.V. Dmytrieva, G. Kosakowski, F.F. Hingerl, K. V. Chudnenko, et al., GEM-Selektor geochemical modeling package: revised algorithm and GEMS3K numerical kernel for coupled simulation codes, Comput. Geosci. V. 17 (No. 1) (2013) 1–24.
[29] B. Lothenbach, F. Winnefeld, Thermodynamic modelling of the hydration of Portland cement, Cement Concr. Res. 36 (No. 2) (2006) 209–226.
[30] B. Lothenbach, F. Winnefeld, C. Alder, E. Wieland, P. Lunk, Effect of temperature on the pore solution, microstructure and hydration products of Portland cement pastes, Cement Concr. Res. 37 (No. 4) (2007) 483–491.